

# The Massive End of the Stellar Mass Function

Richard D’Souza<sup>1\*</sup>, Simona Vegetti<sup>1</sup>, Guinevere Kauffmann<sup>1</sup>

<sup>1</sup>*Max Planck Institute for Astrophysics, Munich, Germany*

Accepted 1988 December 15. Received 1988 December 14; in original form 1988 October 11

## ABSTRACT

We derive average flux corrections to the `Model` magnitudes of the Sloan Digital Sky Survey (SDSS) galaxies by stacking together mosaics of similar galaxies in bins of stellar mass and concentration. Extra flux is detected in the outer low surface brightness part of the galaxies, leading to corrections ranging from 0.05 to 0.32 mag for the highest stellar mass galaxies. We apply these corrections to the MPA-JHU (Max-Planck Institute for Astrophysics - John Hopkins University) stellar masses for a complete sample of half a million galaxies from the SDSS survey to derive a corrected galaxy stellar mass function at  $z = 0.1$  in the stellar mass range  $9.5 < \log(M_*/M_\odot) < 12.0$ . We find that the flux corrections and the use of the MPA-JHU stellar masses have a significant impact on the massive end of the stellar mass function, making the slope significantly shallower than that estimated by Li & White (2009), but steeper than derived by Bernardi et al. (2013). This corresponds to a mean comoving stellar mass density of galaxies with stellar masses  $\log(M_*/M_\odot) \geq 11.0$  that is a factor of 3.36 larger than the estimate by Li & White (2009), but is 43% smaller than reported by Bernardi et al. (2013).

**Key words:** Galaxy Formation – Stellar haloes

## 1 INTRODUCTION

The stellar mass function of galaxies is a basic probe of galaxy formation and evolution enabled by large redshift surveys. In recent years, major advances have been made by large redshift surveys, such as the 2dF Galaxy Redshift Survey and the Sloan Digital Sky Survey (SDSS), in estimating the stellar mass function in the low-redshift Universe (Cole et al. 2001; Bell et al. 2003; Blanton et al. 2003). For example, Li & White (2009) have used a uniform sample of almost half a million galaxies from SDSS DR7 to derive the stellar mass function at  $z = 0.1$ . This has been complemented by the effort of the Galaxy and Mass Assembly Survey (GAMA Baldry et al. 2012), which has accurately constrained the faint end slope of the stellar mass function down to stellar masses  $\sim 10^8 M_\odot$ .

The calculation of the stellar mass function hinges on the proper determination of the stellar mass of a galaxy, which in turn depends critically on the estimation of its total flux in a given pass-band. Systematic differences in the estimation of the stellar mass of a galaxy may arise from different choices of the initial mass function (IMF) and the stellar mass-to-light ratio (M/L), as well as from different estimations of the galaxy total flux. Determining the flux accurately for a large number of galaxies in an all-sky survey

is a challenging task. In particular, quantifying the flux in the outer low surface brightness (LSB) regions of a galaxy has proven to be difficult and is still subject of much debate (Bernardi et al. 2013; Simard et al. 2011). These uncertainties mean that the slope at the massive end of the mass function is not very well determined. This has significant implications for several astrophysical problems, including halo occupation models, the mean baryon fraction in the Universe, X-ray and Sunavev-Zeldovich studies of high mass galaxies, and understanding the evolution of massive galaxies to high redshifts.

Different approaches have been employed by SDSS in its photometric pipeline (`PHOTO`) to estimate the total flux of a galaxy. In addition to SDSS `Petrosian` magnitudes, two dimensional models (e.g. exponential or de Vaucouleurs) have been used to model the surface brightness distribution of galaxies (SDSS `Model` magnitudes). Further improvement has been provided by SDSS `cModel` magnitudes, for which fluxes are estimated as a linear combination of an exponential and a de Vaucouleurs model. In recent years, several studies have tried to fit Sérsic and multi-component models to the surface brightness distribution (Simard et al. 2011; Lackner & Gunn 2012; Bernardi et al. 2013).

Each of these approaches provides a progressively better estimate of the total flux of a galaxy, but they all suffer from the same intrinsic drawback, namely that the models are fits to the central, high signal-to-noise ratio (SNR) regions

\* E-mail address: rdsouza@mpa-garching.mpg.de (RDS)

of the galaxy and assumptions are required about the outer lower SNR (beyond  $\mu_r \sim 27$  mag arcsec $^{-2}$ ) part of the galaxy profile. Additionally, the total flux estimated through model fitting can be biased in a number of ways.

The biggest source of systematic bias in the flux determination is related to the estimation of the sky background, especially for large nearby objects or those located in dense environments (von der Linden 2007; Bernardi et al. 2007). In principle, this can be overcome by considering extremely large fields of view. For example, considerable progress has been achieved by Blanton et al. (2011) by fitting the masked sky background for each SDSS scan with a smooth continuous function.

However, even with improvements to the sky background algorithm, one is still limited by the depth of the survey. The relatively short exposure time of SDSS (53.9 secs) limits the accuracy of the background determination and subtraction. This in turn limits one’s ability to distinguish between the flux of the outer stellar halo and the sky background, leading to an over- or under-estimation of the total flux of a galaxy. In particular, multi-component model fitting of the main galaxy can lead to biased results. This may explain why recent attempts to trace the low SNR LSB part of a galaxy through fitting multi-component models to single SDSS photometric images have yielded divergent results (Simard et al. 2011; Bernardi et al. 2013; Meert et al. 2015).

Other sources of systematic error in determining the flux of a particular object are the procedures employed for deblending and masking, as well as the radial extent of the models used for the surface brightness fitting. Finally, in addition to photometry, several other effects have a considerable impact on the massive end of the stellar mass function, such as evolutionary corrections and *fiber collisions* (i.e. the fraction of galaxies not targeted for spectroscopy due to the fact that fibres cannot be positioned closer together than 55 arcseconds on the SDSS plug plates).

An alternative but viable approach to fitting models to individual images of galaxies, is to stack images of similar galaxies to quantify the average total amount of extra light in the outer parts (Tal & van Dokkum 2011; D’Souza et al. 2014). By stacking galaxies as a function of their stellar mass and galaxy-type, D’Souza et al. (2014) have reached a depth of  $\mu_r \sim 32$  mag arcsec $^{-2}$ . The increased depth of galaxy stacks helps to reliably constrain the total amount of light especially in the LSB component. In addition, the background for stacked galaxies can be determined more accurately. This then provides a direct handle on the corrections to the `Model` magnitudes as a function of the stellar mass and galaxy type.

In this paper, we attempt to derive flux corrections to the `Model` magnitudes and re-derive the galaxy stellar mass function at redshift  $z = 0.1$  using MPA-JHU (Max-Planck Institute for Astrophysics & John Hopkins University) stellar masses (Kauffmann et al. 2003) and the sample of Li & White (2009). We estimate corrections to the `Model` magnitudes by stacking volume-limited samples in bins of stellar mass, concentration and model type. We also consider various effects that may systematically bias the stellar mass function.

In Section 2, we define the samples used for deriving the corrections as well as the full sample used to derive the

stellar mass function. In Section 3, we derive the flux corrections to the `Model` magnitudes. In Sections 4 and 5, we derive the galaxy stellar mass function and the luminosity function respectively. In Sections 6 and 7, we summarise and discuss our results. Throughout this paper, we assume a flat  $\Lambda$ CDM cosmology,  $\Omega_m = 0.25$  and  $\Omega_\Lambda = 0.75$ . We further assume a Hubble parameter  $h = 0.72$  for the calculation of physical distance scales wherever necessary.

## 2 SAMPLE SELECTION

### 2.1 Sample for Calculating the Mass Function

Following Li & White (2009), we select SDSS spectroscopic galaxies from the NYU-VAGC (New York University - Value Added Catalogue)<sup>1</sup> catalogue (Blanton et al. 2005) with redshifts in the range  $0.001 \leq z \leq 0.5$  and *Petrosian*  $r$ -band magnitudes in the range  $12 \leq m_{rPet} \leq 17.6$ .<sup>2</sup> This gives us a total of 533442 galaxies, which are ideal for large scale structure studies. We further pruned the sample to 523476 galaxies by retaining only those galaxies with a valid MPA-JHU stellar mass. We estimate the “effective” survey area to be  $6570 \text{ deg}^2$  (2.0084 steradians), by taking into account the incompleteness and the masked-out regions (due to bright stars) of the survey.

For the stellar mass function, we use the stellar masses provided in the DR7 version of the MPA-JHU catalogue<sup>3</sup>, which assumes a universal Chabrier initial stellar mass function (Chabrier 2003).

To derive the luminosity function, we use the  $r$ -band absolute `Model` magnitude ( $M_{r,0.1}$ ), corrected for evolution and  $K$ -corrected to its value at  $z_0 = 0.1$  according to the following equation:

$$M = m - DM(z) - K(z; z_0) + Q_e(z - z_0), \quad (1)$$

where  $M$  is the absolute magnitude,  $DM(z)$  is the distance modulus at redshift  $z$ ,  $m$  the apparent magnitude,  $K(z; z_0)$  is the  $K$ -corrections relative to a passband blue-shifted by  $z_0$  and the luminosity  $e$ -correction is parametrised linearly by  $Q_e$ . The  $K$ -corrections were calculated using the code `Kcorrect v4_3` (Blanton & Roweis 2007). In general, we assume a uniform luminosity evolutionary correction of  $Q_r = 1.62$  as derived by (Blanton et al. 2003).

### 2.2 Sample for Determining the Flux Corrections

To derive the corrections to the `Model` magnitudes, we stack volume-limited sub-samples of isolated galaxies defined from the parent sample in various ranges of stellar mass, concentration ( $R90/R50$ ) and redshift (See Table 1). In each sub-sample, galaxies that were better fit by an exponential (`Exp`) or a de Vaucouleurs (`deV`) model by the SDSS pipeline (defined by comparing the likelihood values of the model fits from the SDSS `PhotoObjAll` database) were stacked separately.

We select isolated galaxies by requiring that there are no brighter companions in the spectroscopic sample within

<sup>1</sup> Available at <http://sdss.physics.nyu.edu/vagc/>.

<sup>2</sup> We also include the three survey strips in the Southern Cap.

<sup>3</sup> Available at <http://www.mpa-garching.mpg.de/SDSS/DR7/>

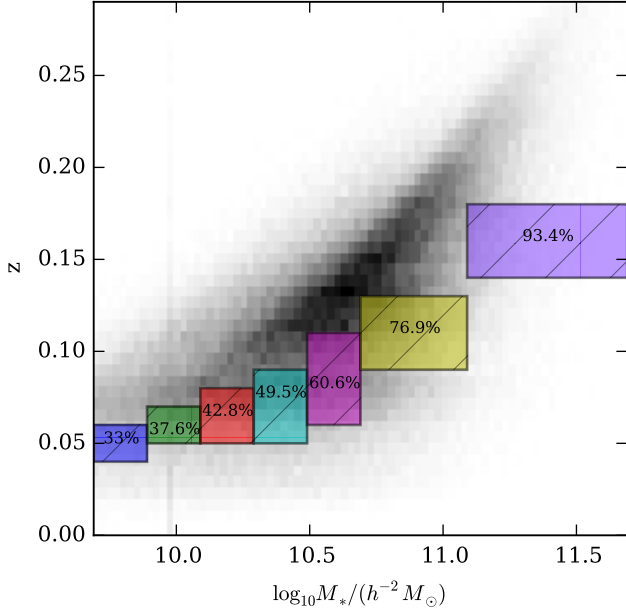


**Figure 1.** Volume-limited samples used for stacking: Shaded contours show the distribution of the parent sample galaxies in the plane of stellar mass versus redshift. The seven coloured boxes indicate the redshift limits of the seven stellar mass sub-samples. These sub-samples are further divided by concentration ( $C$ ) (not shown in the figure). The numbers in the coloured boxes indicate the fraction of centrals in these volume limited stellar mass sub-samples.

$R \leq 1$  Mpc (where  $R$  is the projected comoving separation) and  $|\delta z| < 1000 \text{ km s}^{-1}$ .

In Figure 1, the redshift limits of the various stellar mass sub-samples are shown projected along the plane of stellar mass versus redshift of the parent NYU-VAGC sample. The fraction of centrals in each stellar mass sub-sample are also shown.

### 3 FLUX CORRECTIONS TO THE MODEL MAGNITUDES

In this section, we derive corrections to the original SDSS `Model` magnitudes derived from the standard DR7 photometric pipeline (`photo v5_4`). We first demonstrate that the original SDSS `Model` magnitudes are biased, in agreement with other studies (Simard et al. 2011; Bernardi et al. 2013). We then proceed to derive corrections to the `Model` magnitudes.

#### 3.1 Systematic Biases in Model magnitudes

The original `Model` are affected by two sources of systematic bias related to over-subtraction of the sky background (von der Linden 2007; Bernardi et al. 2007) and to simplistic choices of the model for the surface brightness profile of the galaxy (exponential or de Vaucouleurs). In this section, we allow for more complex models to describe the light profiles and we also allow the sky background to vary.

We fit 2D axisymmetric models (single Sérsic and double Sérsic models along with a constant background) using the Bayesian analysis described by D’Souza et al. (2014) to individual postage-stamp cutouts of the highest stellar mass and high-concentration galaxies ( $11.49 < \log(M_*/M_\odot) < 11.69$ ,  $2.9 < C < 3.3$ ) in the redshift range  $0.14 < z < 0.18$  (covered by the sample G4 above - 38 galaxies) and  $0.2 < z < 0.4$  (414 galaxies). The choice of the sample was motivated by the idea of testing the robustness of the `Model` magnitudes in the limits of high stellar mass and high redshift, where the relative contribution due to the sky background becomes increasingly significant.

We compare our best fitting model with the `Model` magnitudes reported by the SDSS `photo v5_4` pipeline. In Figure 2, we plot a histogram of  $M_{model} - M_{fit}$  for each galaxy. The distribution is broad with a standard deviation of 0.25 magnitudes and is positively skewed. The median is shifted by 0.03 magnitudes and the mean by 0.08 magnitudes. The large spread in the histogram arises from a degeneracy between the best-fit model and the level of sky background. The results in Figure 2 demonstrate that shallow single-exposure SDSS images are insufficient to accurately quantify the total amount of light in massive early-type galaxies to better than 0.25 mag. We also note that estimates of the total flux from a single SDSS image will also be affected by the deblending and masking algorithm<sup>4</sup>.

Because of the limitations in estimating total fluxes from single SDSS images, we have chosen to correct `Model` magnitudes using *stacked images*, where the increased signal-to-noise ratio better constrains both the model and the level of sky background.

#### 3.2 Stacking images

In order to derive the flux corrections to the `Model` magnitudes, we used the sky-subtracted SDSS Data Release 9 images to create mosaics in the  $g$ ,  $r$  and  $i$  bands centred on each galaxy in the sub-samples defined in Section 2.2. The mosaics extend out to radii of 0.6 - 1 Mpc depending on the stellar mass and redshift range. We follow the stacking procedure outlined in D’Souza et al. (in preparation) and similar to that used by D’Souza et al. (2014). In short, each mosaic was deblended, masked, corrected for galactic extinction (Schlegel et al. 1998), transformed to the highest redshift in that respective bin, rotated so that the major axis of each galaxy is aligned, and then stacked using the truncated-mean algorithm.<sup>5</sup> The  $g$ - and the  $i$ - band images were only used to create the final mask along with the  $r$ -band images. Conservative masking was used. The final stacking was done using the masked and transformed  $r$ -band images.

#### 3.3 Measuring the Total Flux of the Stacked Images

Measuring the total integrated flux of a galaxy stack by fitting a model to its light distribution misses a fair amount

<sup>4</sup> In this paper, we follow the deblending and masking technique outlined in D’Souza et al. (in preparation).

<sup>5</sup> For the truncated-mean stack, we removed 5% of the extreme minimum and maximum values for each pixel.

**Table 1.** Volume-limited samples of isolated galaxies selected by stellar mass from the NYU-VAGC sample for the purpose of stacking

Sample	Stellar mass	Concentration	Redshift	$N_{gal\ Exp}$	$N_{gal\ deV}$
A1	$9.69 < \log(M_*/M_\odot) < 9.89$	$1.7 < C < 2.5$	$0.04 < z < 0.06$	797	117
A2	$9.69 < \log(M_*/M_\odot) < 9.89$	$2.5 < C < 3.3$	$0.04 < z < 0.06$	66	501
B1	$9.89 < \log(M_*/M_\odot) < 10.09$	$1.7 < C < 2.5$	$0.05 < z < 0.07$	1028	175
B2	$9.89 < \log(M_*/M_\odot) < 10.09$	$1.7 < C < 2.5$	$0.05 < z < 0.07$	83	1111
C1	$10.09 < \log(M_*/M_\odot) < 10.29$	$1.7 < C < 2.1$	$0.05 < z < 0.08$	638	15
C2	$10.09 < \log(M_*/M_\odot) < 10.29$	$2.1 < C < 2.5$	$0.05 < z < 0.08$	752	308
C3	$10.09 < \log(M_*/M_\odot) < 10.29$	$2.5 < C < 2.9$	$0.05 < z < 0.08$	121	1499
C4	$10.09 < \log(M_*/M_\odot) < 10.29$	$2.9 < C < 3.3$	$0.05 < z < 0.08$	2	1071
D1	$10.29 < \log(M_*/M_\odot) < 10.49$	$1.7 < C < 2.1$	$0.05 < z < 0.09$	342	38
D2	$10.29 < \log(M_*/M_\odot) < 10.49$	$2.1 < C < 2.5$	$0.05 < z < 0.09$	534	535
D3	$10.29 < \log(M_*/M_\odot) < 10.49$	$2.5 < C < 2.9$	$0.05 < z < 0.09$	89	1468
D4	$10.29 < \log(M_*/M_\odot) < 10.49$	$2.9 < C < 3.3$	$0.05 < z < 0.09$	1	2153
E1	$10.49 < \log(M_*/M_\odot) < 10.69$	$1.7 < C < 2.1$	$0.06 < z < 0.11$	239	74
E2	$10.49 < \log(M_*/M_\odot) < 10.69$	$2.1 < C < 2.5$	$0.06 < z < 0.11$	555	1093
E3	$10.49 < \log(M_*/M_\odot) < 10.69$	$2.5 < C < 2.9$	$0.06 < z < 0.11$	72	1981
E4	$10.49 < \log(M_*/M_\odot) < 10.69$	$2.9 < C < 3.3$	$0.06 < z < 0.11$	-	1867
F1	$10.69 < \log(M_*/M_\odot) < 11.09$	$1.7 < C < 2.1$	$0.09 < z < 0.13$	199	264
F2	$10.69 < \log(M_*/M_\odot) < 11.09$	$2.1 < C < 2.5$	$0.09 < z < 0.13$	303	1510
F3	$10.69 < \log(M_*/M_\odot) < 11.09$	$2.5 < C < 2.9$	$0.09 < z < 0.13$	76	2919
F4	$10.69 < \log(M_*/M_\odot) < 11.09$	$2.9 < C < 3.3$	$0.09 < z < 0.13$	1	4180
G1	$11.09 < \log(M_*/M_\odot) < 11.69$	$1.7 < C < 2.1$	$0.14 < z < 0.18$	6	47
G2	$11.09 < \log(M_*/M_\odot) < 11.69$	$2.1 < C < 2.5$	$0.14 < z < 0.18$	11	220
G3	$11.09 < \log(M_*/M_\odot) < 11.69$	$2.5 < C < 2.9$	$0.14 < z < 0.18$	15	792
G4	$11.09 < \log(M_*/M_\odot) < 11.69$	$2.9 < C < 3.3$	$0.14 < z < 0.18$	3	2794

of light due to the inability of the model to reproduce the bulge/disk component of the inner part of the galaxy. For example, a double Sérsic model can miss upto 0.22 mag near the centre of a galaxy stack. On the other hand, “isophotal” magnitudes are unable to measure the LSB features of the galaxy stack, especially in the low S/N regime.

In order to measure the total integrated light in each stack, we consider, therefore, a hybrid approach between a “model” and an “isophotal” magnitude. In particular, we first fit the large mosaics using two-dimensional axisymmetric double Sérsic models with a flat background using the Bayesian analysis described by D’Souza et al. (2014). During this fit, the inner component is truncated outside a radius equal to  $7R_e$ , while the outer component extends out to infinity. Then, to the flux derived by the double Sérsic model, we add the total residual flux ( $= \text{Data} - \text{Model}$ ) within a circular aperture of limiting radius  $R_{lim}$ , defined as the radius at which the residual flux is maximised. The advantage of this hybrid approach is that the double Sérsic model measures the slow decline of flux into the low S/N regime, while the sum of the residual and model fluxes reproduces the total flux in the high S/N part of a galaxy stack.

In the next subsections, we explore the different factors that may bias our measurements of the total flux of the stack.

### 3.3.1 Bias due to Inaccurate Sky Background Subtraction

The sky residuals in the individual SDSS DR9 images are responsible for some small amount of residual sky background in the final stacks ( $< 4 \times 10^{-4}$  nanomaggies per pixel). We quantify this residual by adding a flat background component as a free parameter of our models (Section 3.3). As shown later in Section 3.3.2, this bias is minimal ( $\leq 0.01$  mag).

For the individual DR9 images, Blanton et al. (2011) quantified the spread in the sky background residuals to be  $\sigma \sim 3.13 \times 10^{-3}$  nanomaggies per pixel. The median bias in the  $r$ -band magnitudes was estimated to be at the most 0.1 mag independent of  $R50$ . In addition, higher stellar mass galaxies are found predominately at higher redshifts in the SDSS spectroscopic sample, limiting the bias in the flux of individual images caused by faulty sky-subtraction.

### 3.3.2 Bias due to Models Used

In order to test how the choice of model may affect the corrections to the total luminosity using the “hybrid” magnitudes, we fit each of our galaxy stack using two-dimensional exponential, de Vaucouleurs, Sérsic and double Sérsic models. Each model also includes a flat sky residual. By comparing the evidences generated from the Bayesian fitting, we find that the double Sérsic models are preferred by more

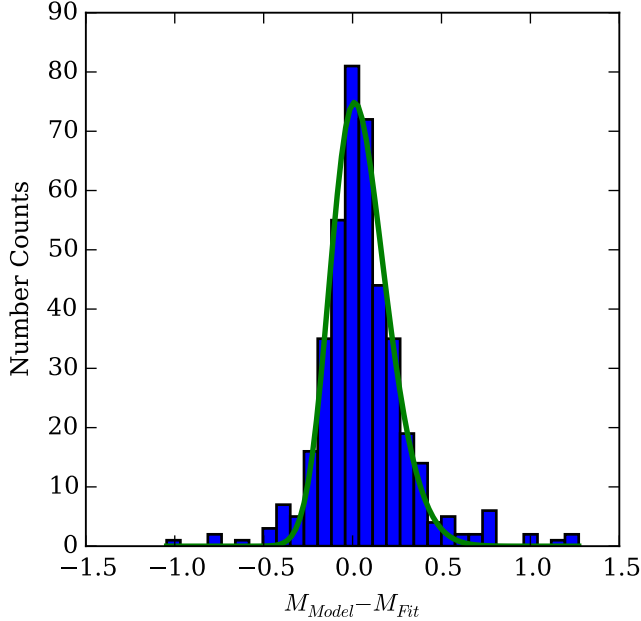


**Figure 2.** Bias in SDSS Model1 magnitudes: A histogram of the difference between the flux derived from our best fit models of high stellar mass high-concentration galaxies and the Model1 magnitudes from DR7 for galaxies with  $11.49 < \log(M_*/M_\odot) < 11.69$ ,  $2.9 < C < 3.3$ ,  $0.14 < z < 0.18$  and  $0.2 < z < 0.4$ . The green solid line indicates the fit to the skewed-normal distribution.

than  $10\text{-}\sigma$  over the other models in all cases. The de Vaucouleur model gives the highest estimate of the total amount of light, followed by the single Sérsic, the double Sérsic and the exponential model respectively. Calculating the magnitudes in the “hybrid” manner as described above gives very little difference in the total flux derived from different models.

Each model also yields different estimates of the residual background in the stacks. However, determining the background level independently and keeping it fixed during the fitting process does not alter our estimates of the extra light (at the 0.01 mag level). This is due to the fact that the results of the fitting are driven primarily by the inner high SNR part of the galaxy stack.

We conclude that the combination of the depth of our stacked image and our “hybrid” magnitudes enables us to accurately constrain the total flux in the galaxy stack. Our outer models are not truncated, but instead extend out to infinity. The difference between models which are truncated at  $7R_e$  and models which instead extend out to infinity is at most 0.05 mag.

### 3.4 Measuring the Flux Corrections

For each stellar mass, concentration range and model fit type (exponential or de Vaucouleurs), we measure the average extra flux correction to the Model1 magnitudes as the difference between the total integrated light in the stack and the median Model1 flux of the galaxies in the stack. The median Model1 magnitude was calculated by taking the median of the

individual fluxes of galaxies in the stack. We find that the median Model1 magnitude is on average higher than the mean Model1 magnitudes. We use a two-dimensional-interpolation scheme to calculate the average extra light as a continuous function of stellar mass and concentration for each model type. These are shown in Figure 3. As can be seen, there is an extra light contribution from those galaxies which were fit by an exponential model both for high concentrations and for high stellar masses. The extra light correction from those galaxies fit by a de Vaucouleurs model comes predominantly from the massive, high concentration galaxies. On the other hand, the de Vaucouleurs model often over-estimates the flux of a galaxy for low concentration massive galaxies.

We note that the large width of the stellar mass bins for the highest stellar mass galaxies may influence the correction derived in the stacking procedure. To account for this, we divide our highest mass sample, G4 ( $11.09 < \log(M_*/M_\odot) < 11.69$ ,  $2.9 < C < 3.3$ ,  $0.14 < z < 0.18$ ), into smaller mass bins of size 0.1 dex. We find that the relative corrections ranges from 0.23 to 0.31 mag, gradually increasing from the lowest to the highest stellar mass bin (see Figure 4). The mean correction derived by stacking the entire sample G4 is 0.29 mag.

For galaxies outside the the mass limits defined in Section 2.2, we extrapolate assuming the same mass corrections of the nearest defined mass bin. In particular, at the high mass end, there are 116 galaxies with stellar masses larger than  $\log(M_*/M_\odot) > 11.69$ , the highest stellar mass bin used above. For these galaxies, we assume the corrections to be the same as found for the highest stellar mass bin (0.31 mag).

Assuming a constant M/L for each galaxy, we calculate the extra mass for each galaxy in our main sample given its stellar mass, concentration and model type (by comparing the likelihoods of the Model1 fits from the SDSS database) as:

$$\log \frac{M_* + \delta M_*}{M_*} = -\Delta \text{Mag} / 2.5 \quad (2)$$

## 4 THE STELLAR MASS FUNCTION OF GALAXIES

### 4.1 Method

We estimate the abundance of galaxies as a function of their stellar mass using the  $1/V_{max}$  method outlined by Li & White (2009). In combination with the depth and the large spectroscopic sample of SDSS, the  $1/V_{max}$  method provides an unbiased estimate of the stellar mass function and its normalisation. In Section 4.2, we demonstrate that the  $1/V_{max}$  estimator is unbiased against large scale structure at stellar masses of  $\log(M_*/M_\odot) \geq 9.5$ , which is the regime studied in this work. We limit ourselves to this regime since as estimated by Figure 4 of Baldry et al. (2008), all galaxies above stellar masses of  $\log(M_*/M_\odot) \geq 9.5$ , will be detected irrespective of their central surface brightness. Moreover, our flux corrections begin from  $\log(M_*/M_\odot) \geq 9.6$  upwards.

For each observed galaxy  $i$ , we define the quantity  $z_{max,i}$  to be the maximum redshift at which the observed galaxy would satisfy the apparent magnitude limit of our sample  $m_{rPet} \leq 17.6$ . Evolutionary and K-corrections are

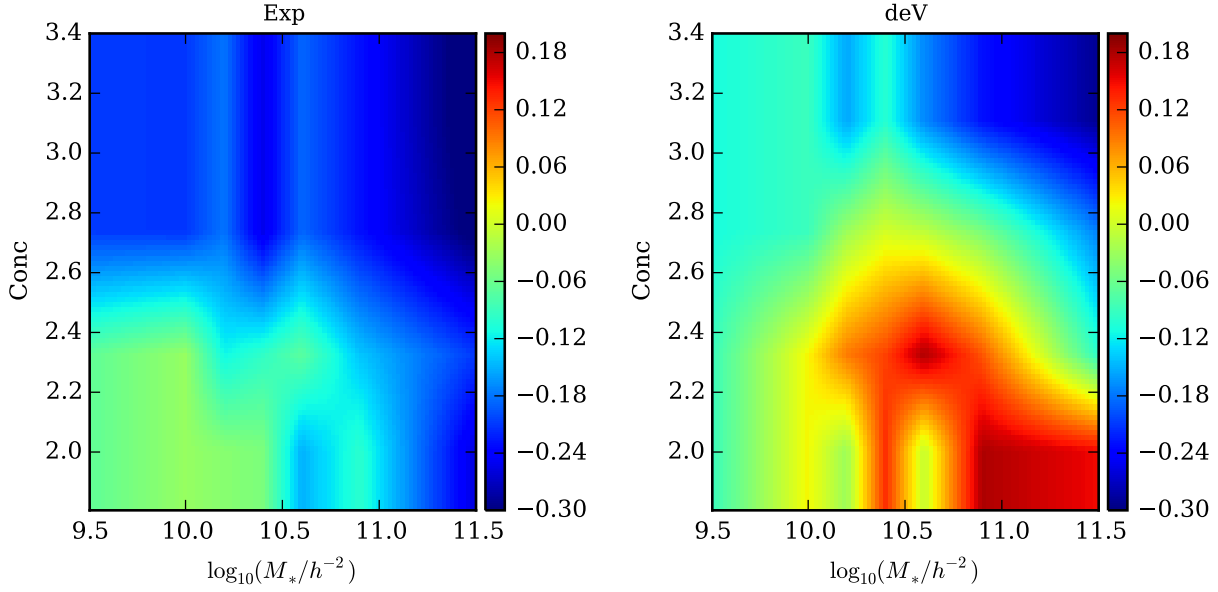


**Figure 3.** The flux corrections ( $\Delta\text{Mag}$ ) as a function of stellar mass and concentration using an interpolation scheme for exponential (Exp) and de Vaucouleurs (DeV) fit galaxies.

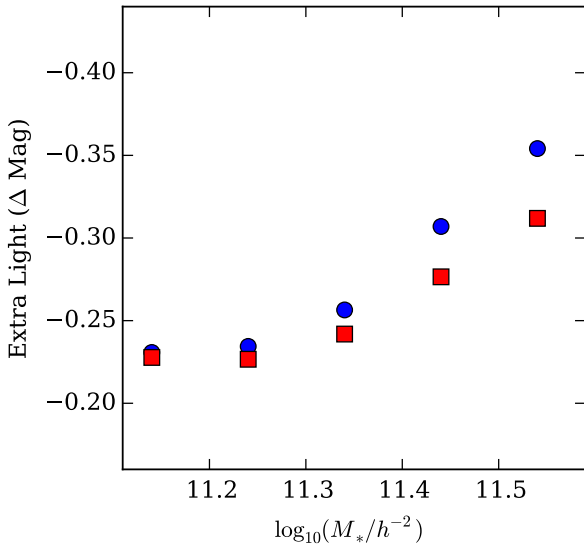


**Figure 4.** The flux corrections ( $\Delta\text{Mag}$ ) as a function of stellar mass for galaxies in the sample G4 (blue circles). We also indicate the uncertainty in the corrections by showing the flux corrections derived from the mean `Model` flux of the stacks (red circles).

included when calculating  $z_{max,i}$ . Hence,  $z_{max,i}$  is the minimum of the upper limit of the redshift slice and the solution of the equation:

$$M_i = m_{rPet}^{Faint} - DM(z_{max}) - K(z_{max}) + Q_e(z_{max} - z_i) \quad (3)$$

Similarly, we also define  $z_{min,i}$  as the minimum redshift at which the galaxy would be present in our sample. Hence,  $z_{min,i}$  is the maximum of the lower limit of the redshift slice and the solution to the equation:

$$M_i = m_{rPet}^{Bright} - DM(z_{min}) - K(z_{min}) + Q_e(z_{min} - z_i) \quad (4)$$

This then allows us to calculate  $V_{max,i}$  for the galaxy in question as the total co-moving volume of the survey between  $z_{min,i}$  and  $z_{max,i}$ . The stellar mass function can be then estimated as:

$$\Psi(M_*)\Delta M_* = \sum_i (f_{norm\ coll,i} V_{max,i})^{-1} \quad (5)$$

where  $f_{norm\ coll,i}$  is the normalised fiber collision factor defined below, and the sum extends over all sample galaxies with stellar masses in the range  $M_* \pm 0.5 \delta M_*$ . The error bars are estimated by taking into consideration both Poissonian and bootstrapping errors, as well as errors due to cosmic variance (See 4.2).

We calculate the stellar mass function in the total redshift range  $0.001 \leq z \leq 0.5$  as well as in three redshift slices:  $0.001 \leq z \leq 0.15$ ,  $0.15 \leq z \leq 0.3$  and  $0.3 \leq z \leq 0.5$ .

## 4.2 Robustness of the $1/V_{max}$ Estimator

In this work, we estimate the abundance of galaxies using the  $1/V_{max}$  method. Given the large effective surface area (nearly  $6570 \text{ deg}^2$ ) and the depth of spectroscopic sample, the  $1/V_{max}$  method will be invariant to large-scale structure up to a limiting stellar mass. To test this, we divide our sample into three independent but contiguous parts (Sample A, Sample B and Sample C split by right ascension), and calculate the standard deviation in the stellar mass function as a

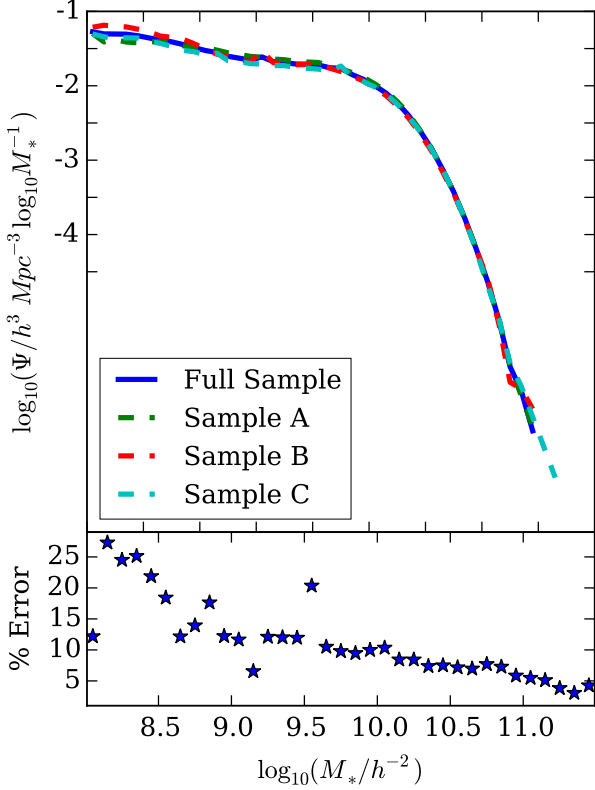


**Figure 5.** Top panel: The stellar mass function for the complete sample as well as the three independent smaller samples A, B and C, using the MPA-JHU stellar masses for the full redshift range  $0.001 \leq z \leq 0.5$ . Bottom Panel: The standard deviation in the stellar mass function as a function of stellar mass.

function of stellar mass. In the bottom panel of Figure 5, the standard deviation is plotted as a function of stellar mass. The difference in the estimates of the stellar mass function due to the  $1/V_{max}$  method from the three independent samples is less than 10% for stellar masses  $\log(M_*/M_\odot) > 9.5$ . The standard deviation gives us also a handle on the errors in our estimates of the stellar mass function due to the cosmic variance.

### 4.3 The Effect of Systematic and Random Errors on the SMF

In calculating the stellar mass function, various systematic and random effects combine to affect the final result. We discuss each of these effects in turn in the following subsections:

#### 4.3.1 MPA-JHU Stellar Masses and Extra light from Photometry

The first source of systematic bias comes from the estimation of the stellar mass of individual galaxies. In this work, we use the MPA-JHU stellar masses to calculate the stellar mass function. This involves a change of flux (from *Petrosian*

to *Model* magnitudes) and M/L ratio (from NYU-VAGC to MPA-JHU) relative to Li & White (2009).

We find that the use of NYU-VAGC stellar masses based on the *Model* magnitudes rather than the *Petrosian* magnitudes introduces a shift beyond the knee of the stellar mass function towards a shallower slope at the higher mass end. This shift is then further increased when we switch to MPA-JHU stellar masses based on the *Model* magnitudes. The slope of the massive end of the mass function is shallower than that obtained by shifting the mass function derived from the NYU-VAGC stellar masses by 0.1 dex (See appendix of Li & White 2009:  $\Delta \log M_* = 0.1$ ). At a stellar mass of  $\log M_* \sim 11.5 M_\odot$ , this accounts for an increase in the stellar mass function by a total of 1.24 dex (a 0.57 dex increase due to the change from *Petrosian* to *Model* magnitudes and a 0.67 dex increase due to the change from the NYU-VAGC to MPA-JHU M/L ratios).

Our assumed M/L ratio affects our estimation of the stellar mass function. The use of the MPA-JHU stellar M/L ratios makes the slope at the massive end shallower than the NYU-VAGC M/L ratios. We note that the MPA-JHU M/L ratios are derived from models that include the possibility of complex star formation histories, whereas the NYU-VAGC assumes that red galaxies can be described by single stellar populations. Analysis of spectra of massive galaxies in the BOSS survey by Chen et al. (2013) indicates that the star formation histories of the most massive galaxies are characterised by episodic star formation histories.

The extra flux derived from the photometry of stacked galaxies introduces a further shift, making the slope at the massive end of the stellar mass function even shallower. We find that this shift of the stellar mass function is independent of whether we apply the corrections only to the central galaxies, or to all the galaxies in the sample. Although a small difference is found at the knee of the mass function, both results are consistent with each other within the error bars.

#### 4.3.2 Fiber Collisions

The second source of systematic bias is caused by fiber collisions. The NYU-VAGC catalogue lists the spectroscopic completeness  $f_{sp}$  of each galaxy, defined as the fraction of photometrically defined target galaxies in the subarea for which usable spectra are obtained. The NYU-VAGC catalogue calculates the average completeness for each of these subareas by taking into consideration overlapping plates. In the jargon of the NYU-VAGC catalogue, these subareas are called *sectors*.  $f_{sp}$  contains information about the missing galaxies due to lack of fibers in dense regions, missing galaxies due to spectroscopic failures, and missing galaxies due to fiber collisions. The average  $f_{sp}$  for the sample defined above is 0.9146. However,  $f_{sp}$  assumes that all galaxies with measured spectra are randomly distributed within a sector, and hence cannot account for specific differences between high and low density regions in the same sector. In particular, due to fiber collisions, certain galaxies (e.g. satellite galaxies of large clusters found at high redshifts) will be preferentially missed.

To account for fiber collisions, we define the fiber collision  $f_{coll,i}$  for each galaxy, as the fraction of photometrically defined target galaxies that fall within a area of  $55''$  in ra-

dius.  $f_{coll,i}$  takes the values between 0.111 and 1.0 (that is, 8 closest neighbours and no neighbours respectively). The average of  $f_{coll,i}$  over our whole sample is 0.93819. We normalise  $f_{coll,i}$  such that its average value is the same as that of  $f_{sp}$ .  $f_{norm\ coll,i} = fac * f_{coll,i}$ , where  $fac$  is defined as  $\langle f_{sp} \rangle / \langle f_{coll} \rangle$  and takes the value 0.9749. The normalised fiber collision  $f_{norm\ coll}$  now has the general average properties of  $f_{sp}$ , but can better account for fiber collisions.

Weighting by normalised fiber collision maintains the normalisation of the stellar mass function at the low mass end and increases the mass function up to 22% at the high mass end. Li & White (2009) did not include fiber collisions in their derivation and we can only reproduce their stellar mass function by using *Petrosian* magnitudes and by neglecting the effect of  $f_{sp}$ .

#### 4.3.3 Evolution Corrections

The third main source of systematic error is related to the assumption about the passive evolution of galaxies both in their number density and luminosity. In order to construct a stellar mass function from a large redshift range ( $0.001 \leq z \leq 0.5$ ), we would need account for the passive evolution of galaxies using a so-called evolutionary correction. Assuming such a uniform evolutionary correction is problematic, since galaxy evolution is a function of galaxy type and cannot be described by a simple linear model. For example, star-forming galaxies will evolve more slowly in luminosity than early-type galaxies.

In order to quantify the effects on the stellar mass function related to the assumptions about galaxy evolution, we consider two approaches. In the first approach, we assume a uniform evolutionary correction ( $Q_r = 1.62$ ), which would represent an upper limit for the evolution of early-type galaxies with high stellar masses and stellar populations that evolve passively with time (i.e. in the absence of any mergers). In the second approach, we derive the stellar mass function without evolution in three redshift slices:  $0.001 \leq z \leq 0.15$ ,  $0.15 \leq z \leq 0.3$  and  $0.3 \leq z \leq 0.5$ .

In Figure 6, we plot the stellar mass function derived using the MPA-JHU stellar masses, including a uniform evolutionary correction, accounting for fiber collisions and for the additional stellar mass corrections due to the extra light at large radii (red solid curve). In addition, we also indicate the mass function calculated in the three redshift slices mentioned above, without evolution. As seen from Figure 6, the evolutionary correction has only a small effect on the stellar mass function ( $\sim 10\%$  at the massive end). This is related to the fact that the luminosity evolution is implicitly folded into the derivation of the M/L ratio.

#### 4.3.4 Uncertainty due to binning the data

Another source of systematic bias is related to binning the data in calculating the mass function via the  $1/V_{max}$  method. In particular, this introduces further uncertainty at the massive end of the mass function due to a combination of the low number statistics and the steep slope of the mass function over this mass range. In order to quantify this uncertainty, we recalculate the mass function with different values for the bin sizes, from 0.05 dex to 0.4 dex. In particular, larger bin sizes tends to bias the slope at the high mass

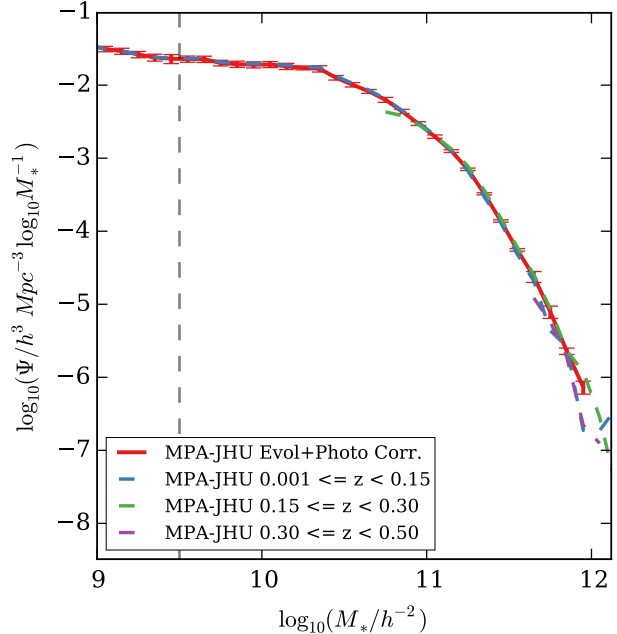


**Figure 6.** The effect of evolutionary corrections on the stellar mass function: The red solid line shows the stellar mass function calculated using MPA-JHU stellar masses corrected for missing light from photometry of stacked galaxies, corrected for fiber collisions and with uniform evolutionary correction  $Q = 1.62$  in the redshift range  $0.001 \leq z \leq 0.5$ . Also plotted are the stellar mass function without evolutionary corrections in redshift slices  $0.001 \leq z \leq 0.15$ ,  $0.15 \leq z \leq 0.3$  and  $0.3 \leq z \leq 0.5$  dashed blue, green and violet lines.

end of the mass function towards shallower values. Reducing the bin size increases the steepness of the slope until a saturation limit of about 0.1 dex. The variation caused by changes in the bin size around the saturation limit is within the uncertainties derived by bootstrapping and within the Poissonian errors. Hence, we calculate the stellar mass function in bins of 0.1 dex.

#### 4.3.5 Eddington Bias

Another source of systematic bias in the stellar mass function is caused by the random errors in the flux and M/L ratios of individual galaxies. Such an “Eddington” bias causes the stellar mass function to be higher in the low-number density part because of scattering from the lower stellar masses (higher number density). This becomes particularly acute because of the steepness of the stellar mass function at higher stellar masses.

To correct for this bias, we assume a parametrized form for the stellar mass function. We convolve this function with a distribution of the uncertainties in the stellar mass. We then fit this convolved function to the binned values of the stellar mass function calculated from the data using a maximum-likelihood method. The best fit parametric function is thus our true stellar mass function corrected for the Eddington bias. For the parametric function, we assume a

**Table 2.** Parameters of a double Schechter function fit to the stellar mass function of SDSS galaxies.

$\Phi^*$ ( $h^3 \text{Mpc}^{-3} \log_{10} M^{-1}$ )	$\alpha$	$\log_{10} M^*$ ( $h^{-2} M_\odot$ )
0.008579	-1.082	10.615
0.000355	-1.120	10.995

double Schechter function, given by

$$\Psi_M dM = \left[ \frac{\Psi_1^*}{M_1^*} e^{-M/M_1^*} \left( \frac{M}{M_1^*} \right)^{\alpha_1} + \frac{\Psi_2^*}{M_2^*} e^{-M/M_2^*} \left( \frac{M}{M_2^*} \right)^{\alpha_2} \right] dM, \quad (6)$$

where  $\Psi_M dM$  is the number density of galaxies between  $M$  and  $M + dM$ . This provides a much better fit to the data relative to a single Schechter. We further assume that the uncertainties in the stellar mass are distributed normally in  $\log_{10}(M_*/M_\odot)$ .

To estimate the uncertainties in the stellar mass, we first estimate the M/L uncertainties as a function of stellar mass from the MPA-JHU database. We find that the average uncertainty  $\Delta \log_{10}(M/L)$  ranges from 0.08 to 0.1 as a function of stellar mass. We then estimate the average uncertainty in the `Model` magnitude as a function of stellar mass. We find that the average uncertainty in the `Model` magnitude is  $\sim 0.02 \text{ mag}$  across the stellar mass range considered. Hence the M/L uncertainty is much larger than the flux uncertainty.

We find that correcting the stellar mass function for the Eddington bias reduces it at the high mass end by as much as 0.48 dex.

#### 4.4 Results: Stellar Mass Function

In Figure 7, we present our final estimate of the stellar mass function corrected for missing flux, fiber collisions, evolution and Eddington bias with that of the original Li & White (2009) in red and the Bernardi et al. (2013) (Sersic-Exp fits) stellar mass function in green.

We provide a parametric representation of the stellar mass function for stellar masses greater than  $\log(M_*/M_\odot) \geq 9.5$ . The parameters of the double Schechter function are listed in Table 2. An integration of our stellar mass function for stellar masses greater than  $\log(M_*/M_\odot) \geq 9.5$  gives the mean comoving stellar mass density of the low redshift universe as  $\phi_* = 3.7 \pm 0.3 10^8 h \text{Mpc}^{-3}$ . This amounts to a 35% increase in the mean comoving stellar mass density contributed from the same stellar mass range for the Li & White (2009) stellar mass function. In particular, focussing on the high stellar mass end: the mean comoving stellar mass density of galaxies with stellar masses  $\log(M_*/M_\odot) \geq 11.0$  is a factor of 3.36 larger than the estimate by Li & White (2009), but is 43% smaller than reported by Bernardi et al. (2013).

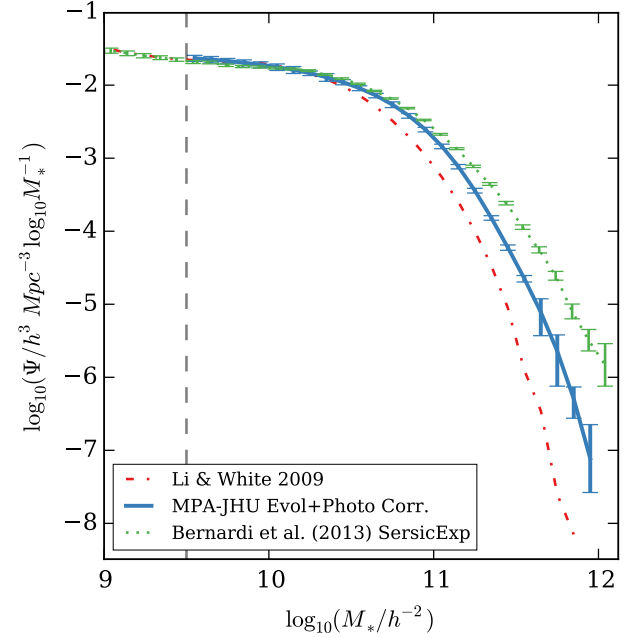


**Figure 7.** The stellar mass function: The blue solid line shows the stellar mass function calculated using MPA-JHU stellar masses, corrected for missing flux, fiber collisions, evolution and Eddington bias. The red dot-dashed line shows the original Li & White 2009 stellar mass function calculated using the NYU-VAGC stellar masses based on `Petrosian` magnitudes. Also shown are the Bernardi et al. (2013) stellar mass function values (green) based on Sersic-Exp fits to individual galaxies. The dashed vertical line indicates our lowest stellar mass limit above which the stellar mass function is not affected by surface brightness completeness issues.

## 5 GALAXY LUMINOSITY FUNCTION

Similar to the galaxy stellar mass function, we also calculate the galaxy luminosity function using the  $1/V_{max}$  method. However, more careful attention needs to be paid to the evolutionary corrections which affects the luminosity function not only via the derivation of  $V_{max}$ , but also via the calculation of a galaxy luminosity via equation 1. We calculate the luminosity function using two approaches: in redshift slices ( $0.001 \leq z \leq 0.15$ ,  $0.15 \leq z \leq 0.3$  and  $0.3 \leq z \leq 0.5$ ) without evolution and using a uniform evolutionary correction of  $Q_r = 1.62$ . In Figure 8, we present the results of  $M_{0.1r}$  band luminosity function considering `Model` magnitudes with photometric corrections from stacking, fiber collisions and evolutionary corrections in bins of 0.25 dex. We also indicate the luminosity function without evolution corrections in three redshift slices. A comparison of our results with those of Bernardi et al. (2013) would require a more careful treatment of luminosity evolution which is beyond the scope of this paper.

## 6 SUMMARY

In this paper, we have shown that stacking similar galaxies together in volume-limited stellar mass and concentration bins allows one to derive average flux corrections to the SDSS `Model` magnitudes. In particular, we find that these

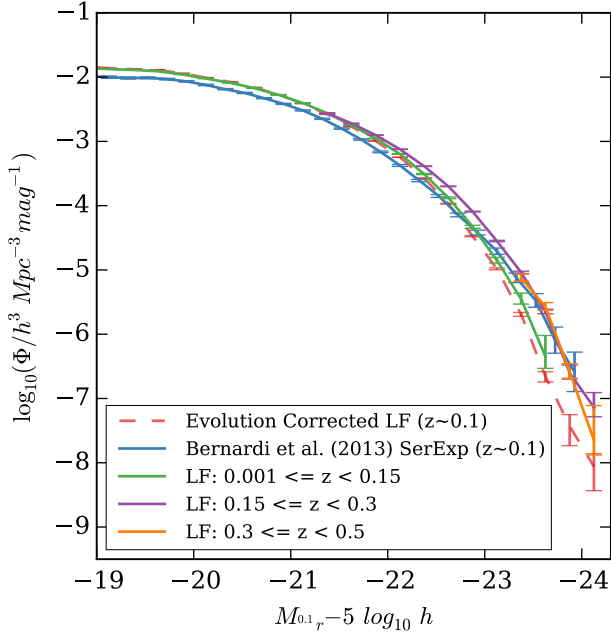


**Figure 8.** The luminosity function: The  $M_{0.1r}$  luminosity function calculated with photometric corrections, fiber collisions and flux uncertainty in three redshift slices and assuming an uniform evolutionary correction of  $Q_r = 1.62$

. We also show the corresponding luminosity function from Bernardi et al. (2013) Sersic-exponential fits.

corrections range from 0.02 to 0.31 magnitude, depending on the stellar mass and concentration of the galaxy.

We apply these corrections to the `Model` fluxes and re-derive the stellar mass function using MPA-JHU stellar masses, accounting for galaxy evolution corrections and fiber collisions. We find that the slope of the massive end of the stellar mass function is shallower than reported by Li & White (2009), but much steeper than derived by Bernardi et al. (2013).

The biggest change in the slope at the massive end of the mass function comes from our adoption of the MPA-JHU stellar masses (as much as a 1.24 dex increase at  $\log M_* \sim 11.5 M_\odot$  with respect to Li & White 2009). This involves an increase of 0.57 dex and 0.67 dex due to the changes in flux and M/L ratio respectively. The second major contributor is the bias caused by the uncertainty in M/L ratio and flux measurements of individual galaxies which accounts for a decrease of  $\sim 0.48$  dex in the mass function at the massive end. Fiber collisions contributes to an increase of nearly 22% at the massive end. Galaxy evolution corrections accounts for a decrease of maximum 10% at the massive end of the mass function.

We also derive the  $r$ -band galaxy luminosity function and obtain similar results. In particular, the biggest source of systematic uncertainty in the galaxy luminosity function is related to the model assumed for the galaxy evolution correction. In this Paper, we use the evolution correction values derived by Blanton et al. (2003), which serves as an upper limit for galaxies at the bright end of the galaxy luminosity function.

## 7 DISCUSSION

The flux corrections to the SDSS `Model` magnitude and their respective uncertainties derived in this work by stacking mosaics of similar galaxies in volume limited stellar mass and concentration bins are consistent with those presented by Simard et al. (2011). We find no evidence for the need of large flux corrections of the order of 0.5 magnitudes as proposed by Bernardi et al. (2013).

Our results are also consistent with extremely deep imaging of nearby early-type galaxies, obtained with the MegaCam camera on the Canada-France-Hawaii Telescope which indicate that outer LSB light contributes 5 to 16 percent to a galaxy’s total luminosity (Duc et al. 2015). Stacking results for luminous red galaxies (average redshift of  $z \sim 0.34$ ) from Tal & van Dokkum (2011) also indicate that typical SDSS-depth images miss about 20 percent of the total stellar light.

A number of systematic differences could contribute to the discrepancy between our results and those by Bernardi et al. (2013). In the limit of low SNR, the determination of the sky background level can influence the measured flux of a galaxy derived from fitting models to the surface brightness distribution. The depth of an image limits ones ability to distinguish between the flux of the outer LSB features of the galaxy and the sky background, especially for large stellar mass galaxies at higher redshifts. The use of multi-component models aggravates this problem.

The simultaneous estimation of the model parameters and the sky background level may be prone to systematic bias, since these are often degenerate with each other. Bernardi et al. (2013) use the `PyMorph` algorithm (based on `GALFIT`), which estimates the galaxy flux based on model fitting along with a simultaneous estimation of the sky background. Meert et al. (2013) and Meert et al. (2015) have already highlighted the effect of a bias in the sky subtraction on the total flux of a galaxy. On the other hand, SDSS `Photo` pipeline estimates the `Model` magnitudes by first independently estimating and subtracting the local sky background. A similar procedure is followed by Simard et al. (2011). In this work, we use the background subtracted images provided with SDSS DR9 to derive the flux corrections. In addition, the depth of our stacked images allows us to accurately determine the residual sky background.

Estimating the total flux of a galaxy is dependent on the exact procedure used for deblending and masking ( see Blanton et al. 2011 and Simard et al. 2011). In particular, the amount of masking employed has a substantial effect on the amount of flux that is derived for a specific galaxy. In this Paper, we use the conservative masking described by D’Souza et al. (2015), which involves using multiple runs of `SExtractor` (Bertin & Arnouts 1996).

Guo et al. (2010) calculated the stellar mass function using the NYU-VAGC stellar M/L ratios and `Model` magnitudes using the methodology of Li & White (2009). The stellar mass function derived here has a large shift and shallower slope than Guo et al. (2010), owing primarily to the use of the MPA-JHU stellar masses and the flux corrections to the `Model` magnitudes. The results of our work will affect the majority of recent halo occupation and abundance matching studies (e.g. Moster et al. 2013) that use the measurements of the stellar mass function from Guo et al. (2010).

Finally, we comment that the majority of studies of the evolution of the massive end of the stellar mass function have found surprisingly little change out to  $z \sim 1$  (Maraston et al 2013; Moustakas et al 2013; Fritz et al 2014). The co-moving number density of galaxies with stellar masses greater than  $10^{11} M_{\odot}$  has apparently remained constant over the past 9 Gyr, calling into question the late build-up of these systems through mergers and accretion. Our work has shown that a significant fraction of the mass of these systems may be “hiding” in low surface brightness outer components that are systematically missed by conventional photometric extraction software. Accurately quantifying the *evolution* of the stellar mass in these halos will be an important challenge for next generation deep imaging surveys.

## ACKNOWLEDGEMENTS

Funding for SDSS-III has been provided by the Alfred P. Sloan Foundation, the Participating Institutions, the National Science Foundation, and the U.S. Department of Energy Office of Science. The SDSS-III web site is <http://www.sdss3.org/>.

SDSS-III is managed by the Astrophysical Research Consortium for the Participating Institutions of the SDSS-III Collaboration including the University of Arizona, the Brazilian Participation Group, Brookhaven National Laboratory, University of Cambridge, Carnegie Mellon University, University of Florida, the French Participation Group, the German Participation Group, Harvard University, the Instituto de Astrofísica de Canarias, the Michigan State/Notre Dame/JINA Participation Group, Johns Hopkins University, Lawrence Berkeley National Laboratory, Max Planck Institute for Astrophysics, Max Planck Institute for Extraterrestrial Physics, New Mexico State University, New York University, Ohio State University, Pennsylvania State University, University of Portsmouth, Princeton University, the Spanish Participation Group, University of Tokyo, University of Utah, Vanderbilt University, University of Virginia, University of Washington, and Yale University.

## REFERENCES

- Baldry I. K., Driver S. P., Loveday J. et al., 2012, MNRAS, 421, 1621
- Baldry I. K., Glazebrook K., Driver S. P., 2008, MNRAS, 388, 945
- Bell E. F., McIntosh D. H., Katz N., & Weinberg M. D. 2003, ApJS, 149, 289
- Bernardi M., Hyde J. B., Sheth R. K., Miller C. J. et al. 2007, AJ, 133, 1741
- Bernardi M., Meert A., Sheth R. K., Vikram et al. 2013, MNRAS, 436, 697
- Bertin E., & Arnouts S. 1996, AAPS, 117, 393
- Bertin E., Mellier Y., Radovich M., et al. 2002, ASPC, 281, 228
- Blanton M. R., Hogg D. W., Bahcall N. A., et al. 2003, ApJ, 592, 819
- Blanton M. R., Schlegel, D. J., Strauss, M. J., et al. 2005, ApJ, 129, 2562
- Blanton M. R., Eisenstein D., Hogg D.W., Schlegel D.J., Brinkmann, J. 2005, Apj, 629, 143
- Blanton M. R., Roweis S. 2007, AJ, 133, 734
- Blanton M. R., Kazin E., Muna D., Weaver B. A., & Price-Whelan, A. 2011, AJ, 142, 31
- Chen Y., Kauffmann G., Heckman T. M., Tremonti C., et al. 2013, MNRAS, 429, 2643
- Cole S., Nøberg P., et al. 2001, MNRAS, 326, 1, 255
- D’Souza R., Kauffmann G., Wang J., Vegetti S. 2014, MNRAS
- D’Souza R., Kauffmann G., Vegetti S. 2015, (in preparation)
- Duc P., Cuillandre J., Karabal E., Cappellari M., 2015, MNRAS, 446, 120
- Fritz A., et al., 2014, A&A, 563, A92
- Guo Q., White S., Li C., Boylan-Kolchin M., 2010, MNRAS, 404, 1111
- Kauffmann G., Heckman T. M., White S. D. M., et al. 2003, MNRAS, 341, 33
- Kauffmann G., White S. D. M., Heckman T. M., et al. 2004, MNRAS, 353, 713
- Kelvin L.S., Driver S.P., Robotham A.S.G., Hill D. T. et al. 2012, MNRAS, 421, 1007
- Lackner C. N., & Gunn J. E. 2012, MNRAS, 421, 2277
- Li C., White S. D. M. 2009, MNRAS, 398, 4, 2177
- Maraston C., et al., 2013, MNRAS, 435, 2764
- Meert A., Vikram V., Bernardi M., 2013, MNRAS, 433, 1344
- Meert A., Vikram V., Bernardi M., 2015, MNRAS, 446, 3943
- Mendel, J. T., Simard L., Palmer M., Ellison S.L., Patton D.R., 2014, ApJS, 210,3
- Moustakas J., et al., 2013, ApJ, 767, 50
- Schlegel D. J., Finkbeiner D. P., & Davis M. 1998, ApJ, 500, 525
- Simard L., Mendel J. T., Patton D. R., Ellison S. L., McConnell A. W., 2011, ApJS, 196,11
- Tal T., & van Dokkum P. G. 2011, ApJ, 731, 89
- Von Der Linden A., Best P.N., Kauffmann G., White S.D.M., 2007, MNRAS, 379, 867